4.1 Introduction

The mesoporous ceramics are important materials extensively used for biomaterials, catalysis support, thermal insulation, filters, light-weight structural material, and for fire protection. It has several unique properties, such as high porosity (70 to 90%), low density (0.3 to 0.7 gm/cc), high surface area, low thermal conductivity, and high thermal stability (Tang *et al*., 2004) compared to conventional dense ceramics. Several processing methods have been developed for the fabrication of porous ceramics include freeze-casting (Verma *et al*., 2015), gelation foaming (Tomita and Kawasaki, 2005), starch-consolidation (Lyckfildt and Ferreira, 1998), direct casting (Dhara and Bhargava, 2005), sol-gel reaction and mechanical foaming (Tomita and Kawasaki, 2004; Kim *et al*., 2013). However, most of the fabrication process of foam generates a huge volume of greenhouse gases during firing by the decomposition of organic compounds or volatile matter present in the raw materials. These greenhouse gases affect global warming and create a barrier to the production of ceramic foams regarding the environmental point of view. Present work deals with the sustainable routes for the fabrication of ceramic foams like silica and mullite foam using waste rice husk ash (RHA) without using any foaming agents or additives.

In the recent years, silica foams are extensively used for the adsorption media (Vilarrasa-García *et al*., 2014), drug delivery (Quiño *et al*., 2018), chromatography (Ahmed *et al*., 2012), and catalysis (Iwamoto *et al*., 2003); due to their good physical (pore size, pore volume, and surface area) properties. Therefore, several researchers have introduced numerous routes and sources of silica for the fabrication of silica foam. Tomita and Kawasaki *et al*. (2004) has prepared silica foam by the sol-gel reaction and mechanical foaming methods using silica sol (~30 wt.% SiO_2) as the silica source. García *et al*. (2014) have prepared mesocellular silica foams by the hydrothermal route and using tetraethyl orthosilicate (TEOS) as a silica source. Chen *et al*. (2017b) have fabricated hollow silica microspheres through a hard-template method in which they have used colloidal carbon, cetyltrimethylammonium

bromide (CTAB) and TEOS as a template, modifying agent and silica source, respectively. Verma *et al.* (2013) have synthesized silica foam through steam heating route, where fused silica powder, ovalbumin, and sucrose are used as a silica source, binder and additive, respectively.

Porous mullite ($3Al_2O_3{\cdot}2SiO_2$) ceramics have also acquired great attention in different advanced applications, e.g., bio-scaffolds, acoustic, thermal insulation, high-temperature filters, burners, and catalyst supports, etc. (Ge *et al.*, 2018; Pyzik *et al.*, 2011; Hammel *et al.*, 2014). It has some excellent properties, like low thermal conductivity and thermal expansion coefficient, good hot mechanical strength and thermal shock resistance, high melting point, and excellent corrosion resistance (Schneider *et al.*, 2008; Talou *et al.*, 2015; Wang *et al.*, 2016). However, mullite foams are synthesized using the commercial-grade high-purity mullite powder (Talou and Camerucci, 2010; Qian *et al.*, 2014; Talou *et al.*, 2015; Deng *et al.*, 2015; Ge *et al.*, 2018) or expensive reagents like aluminum isopropoxide ($C_9H_{21}AlO_3$) (Ding *et al.*, 2007), aluminium hydroxide ($Al(OH)_3$) (Li *et al.*, 2018) as Al_2O_3 sources, along with silica fume (Du *et al.*, 2016) and colloidal silica as SiO_2 sources. Moreover, different other chemicals, e.g., acrylamide, polyacrylic acid sodium, sodium lignin sulfonate, acetoglyceride, sodium carboxymethyl cellulose, etc. are also used as monomers, cross-linker, pore former, catalyst and curing agent (Qian *et al.*, 2014; Du *et al.*, 2016). Thus, researchers are looking to find low-cost ingredients for the industrial-scale production of mullite foams. Wang *et al.* (2016) have fabricated the mullite foams using coal-series kaolin, which is a special coal gangue (by-product of coal mining). Zhou *et al.* (2018) have used low-cost white clay and industrial alumina for the preparation of porous mullite ceramics. Chen *et al.* (2016) have synthesized the mullite membrane using waste coal fly ash and natural bauxite powder for waste-water treatment.

Slip-casting is a ceramic processing technique, which is mainly used for making pottery. In slip-casting, a liquid-solid mixture is poured into the plaster moulds and the liquid

from the mixture is wicked into the pores through the capillary action. A layer of solid mass is formed inside the walls of the mould after water removal (Ceramic Processing: Slip Casting, 2014).

This study investigates the possibility of using RHA extracted nano-silica and sol for the fabrication of silica and in-situ mullite foam without the addition of any additives or foaming agents. This research also studies the effect of different compactions on the physical and mechanical performance of the silica foams with different foam-forming temperatures. The present study is a novel approach to investigate the ability of a slip-casting method for the preparation of in-situ mullite foams using RHA derived sol as a silica source. The physico-mechanical and thermal conductivity characteristics of the synthesized mullite foams are comprehensively examined. The obtain properties of the waste-derived foam samples are compared with the other process derived porous ceramic systems.

4.2 Experimental procedure

4.2.1 Silica foam synthesis

The most facile and green technology, i.e., low compaction on the semi-wet nano powder was adopted for the synthesis of silica foam specimens. The sample's nomenclatures, a variation of compaction, and synthesis temperature were tabulated in Table 4.1. 3 wt.% of water was mixed with RHA derived silica, and mixing was done for 5 min. Then, the semi-wet powder was pressed by the uniaxial hydraulic press at two different pressures, i.e., 31.20 and 62.40 MPa (0.25 and 0.50 tons load on 10 mm diameter samples). The pressed silica pallets were heat-treated at 400, 500, 550, and 600°C in air for 30 min with a heating and cooling rate of 1ºC/min. For appropriate results, five specimens of each sample were prepared.

Table 4.1 Sample's nomenclature, variation of compaction and foaming temperatures for silica foams.

Samples	f-1	f-2	f-3	f-4	f-5	f-6	f-7	f-8
Pressure (MPa)	31.20	62.40	31.20	62.40	31.20	62.40	31.20	62.40
Temperature (°C)	400	400	500	500	550	550	600	600

4.2.2 Mullite foam synthesis

The preparation scheme of mullite foam is depicted in Figure 4.1. Mullite ($3Al_2O_3 \cdot 2SiO_2$) foam was prepared by a facile and green route, i.e., slip-casting. Therefore, stoichiometric (3:2) molar ratio of reactive alumina and silica (7.5 wt.% solid containing RHA derived sol) was mixed in a container (without adding extra water) with sodium silicate solution as deflocculant (0.5 wt.%). The mixing was performed for 4 h with 200 rpm, and the smooth slurry of alumina-silica was formed. The slurry was poured into the different shape of the cavity of the plaster of paris (POP) mould and the POP was then started to absorb the water from the slurry. The layer of alumina-silica mixture mass was constituted inside into the cavity of the POP mould. After removing water from the slurry, the mould was left for 6 h to dry the casted mass at room temperature. Later, the casted solid mass was taken away from the mould and dried at 110°C for 10 h in an air oven. The dry casted mass was then fired at 1100°C, 1200°C, 1250°C, 1300°C, 1350°C and 1400°C for 2 h with heating and cooling rate 2ºC/min in the air atmosphere.

Figure 4.1 Preparation scheme of mullite foam.

4.3 Results and discussion

4.3.1 Characterization of RHA derived silica

The room temperature XRD pattern of RHA extracted silica powder is shown in Figure 4.2(a). It represents only a broad and wide peak between 15° to 35°, centered at around 22°, which demonstrates the presence of silica (JCPDS 47-0715) (Mor *et al.*, 2017). However,

the absence of any sharp diffraction peak confirms its amorphous nature (Gu *et al*., 2015; Sixiao, and Hsieh, 2014). The chemical composition of the silica contains above 99 wt.% of SiO_2, as shown in Table 4.2.

Table 4.2 The chemical composition of RHA derived silica.

Compounds	SiO_2	Na_2O	P_2O_5	K_2O	CaO	Fe_2O_3	TiO_2	MgO
wt.%	99.32	0.31	0.11	0.08	0.07	0.05	0.02	0.04

Figure 4.2(b) illustrates the FTIR spectrum of as-prepared nano powder. It indicates the presence of characteristic bond of the silicate system at around 1064 cm^{-1}, which represents the asymmetric stretching vibration of siloxane (Si–O–Si) bonds (Cui *et al*., 2015b; Farshid *et al*., 2013). The peaks around 790 and 445 cm^{-1} are ascribed to the symmetric stretching and bending vibrations of the Si–O bonds, respectively (Mor *et al*., 2017, Xiao *et al*., 2015). The broad absorption peaks between 3100 and 3600 cm^{-1} are related to the silanol group (Si–OH) and stretching vibration of the adsorbed water (H–O–H) on the silica surface (Shahnani *et al*., 2018; Cui *et al*., 2015b). The small peak at around 1630 cm^{-1} corresponds to the bending vibrations modes of adsorbed water molecules (Rafiee and Shahebrahimi, 2012; Velmurugan *et al*., 2015). No other peaks have been detected between 1700 and 2750 cm^{-1}, which suggests that no other compounds like NaCl, alkaline earth metals, alkali, organic elements, and other impurities are present in the system (Mor *et al*., 2017).

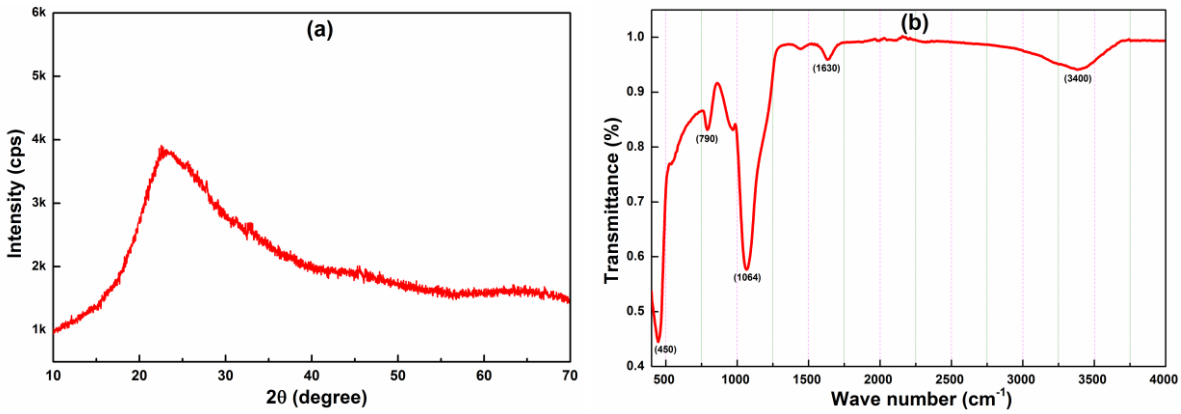

Figure 4.2 (a) XRD and (b) FTIR spectrum of RHA extracted silica.

SEM micrograph of the alkali extracted silica from RHA is shown in Figure 4.3(a). It indicates that the silica particles are highly agglomerated, and the average size is less than 50

nm. The surface to volume ratio of silica nano particles (NPs) is high. It may help to enhance the strong, attractive, cohesive forces between the particles compared to gravitational forces (Min *et al*., 2007). Therefore, silica NPs are agglomerated. The EDX study of the silica is presented in Figure 4.3(b), and it exposes the quantitative existence of Si and O elements with their nearly respective proportions in silica. No impurity element was found within the accuracy limit of the EDX instrument. It confirms that the RHA extracted nano silica through the alkali extraction method is highly pure. Silica NPs extracted from RHA are also characterized in terms of specific gravity by the Archimedes principle through RD bottle method. The specific gravity of silica NPs is found at about 1930 kg/m^3.

The size, shape, and internal structure of RHA derived silica can more correctly be described through the TEM analysis, as shown in Figure 4.3(c). It is seen that the particles are nearly spherical in shape with huge agglomeration. It may occur due to the presence of the bridge bonding of silicon-oxygen in the system (Le *et al*., 2013). The particle's diameter of the silica is between 10 to 30 nm. The selective area electron diffraction (SAED) pattern of SiO_2 powder indicates that the structure of the silica is amorphous due to the absence of intensities ring in the diffraction pattern. It is also confirmed by the XRD analysis of SiO_2 (Figure 4.2(a)).

The DTA and TGA curve of the silica NPs up to 800°C is presented in Figure 4.4. The DTA curve shows two distinct endothermic peaks from room temperature to 500°C. The first peak around room temperature to 130°C may be ascribed to the removal of physically absorbed water from the surface of silica NPs. At high temperature, around 250 to 500°C an endothermic peak is detected due to the breaking of the hydrogen bond, which is presented as a Si–OH (Liu *et al*., 2007). Therefore, around 12 wt.% of total mass loss is associated in TGA curve. It can be attributed to two kinds of water removal. No further changes are observed up to 550°C. Subsequently, a small exothermic peak at around 570°C is detected in the DTA

curve, without any weight loss, and it may be ascribed to the crystallization of amorphous nano-silica.

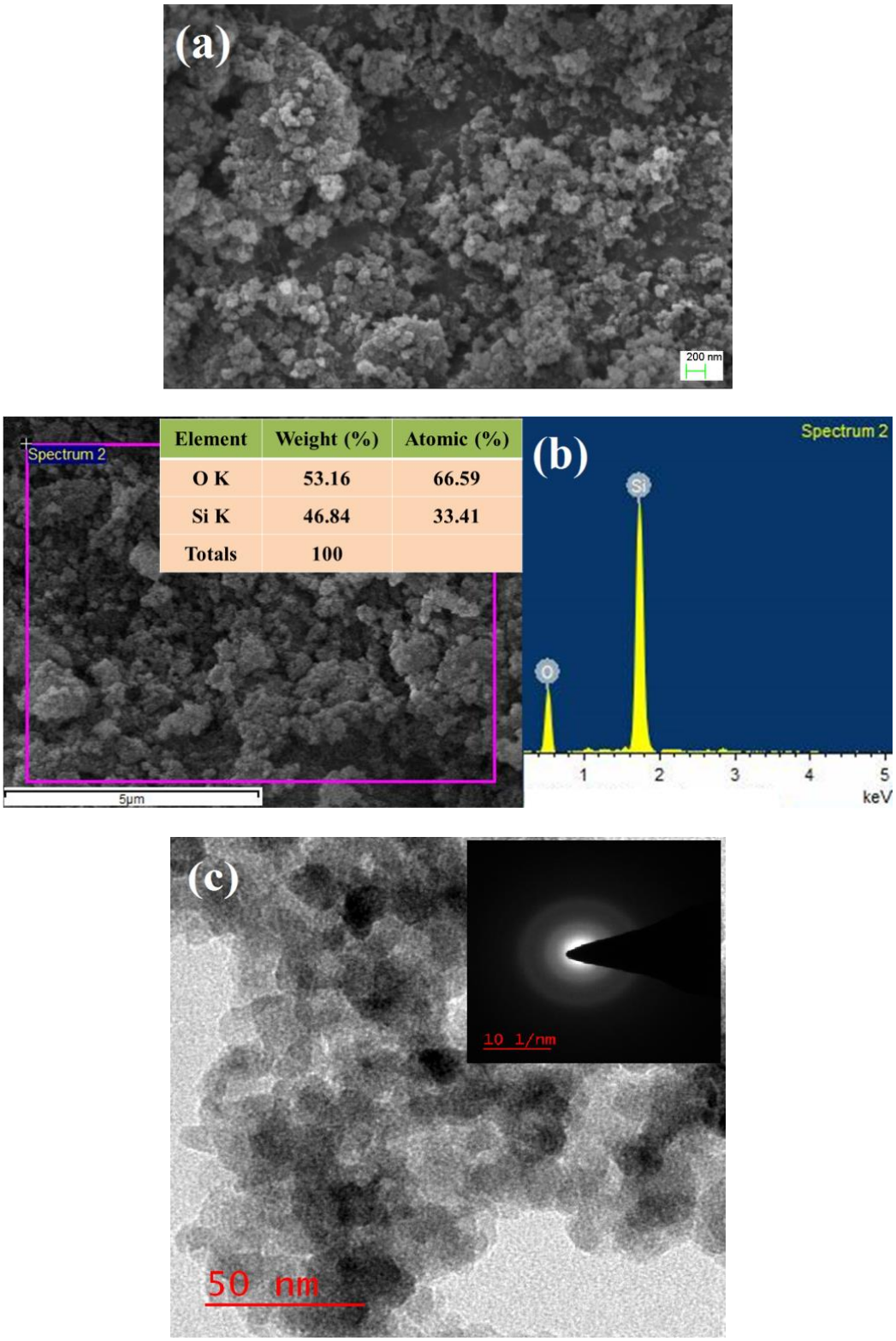

Figure 4.3 (a) SEM, (b) EDX and (c) TEM image of silica nano particles.

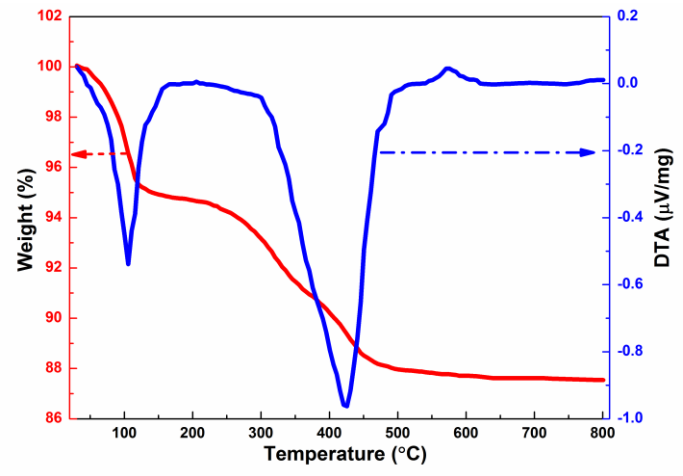

Figure 4.4 DTA-TGA analysis of RHA derived silica.

In recent years, silica NPs have acquired much attention due to several applications in different fields, like medical, catalysis, additives in plastics, polymer, and rubber; solar cells, electronics, thermal insulators, and concrete (Alshatwi *et al*., 2015). However, commercially available high purity (>99%) nano-silica (10 to 50 nm) is expensive. Therefore, researchers are trying to find out the alternative route to fabricate low-cost high purity nano silica. Waste RHA derived high purity nano size amorphous silica containing sol is environmentally and economically benign. Moreover, alkali extraction route derived silica sol from RHA is economical due to low synthesis temperature (90°C) and inexpensive raw materials. It has no tendency to generate any greenhouse gases like CO_2 during the sol extraction. Other possible gases like hydrochloric (HCl ↑) or chlorine (Cl ↑) are transformed into NaCl through the equation 3.2. Table 4.3 shows the cost comparison between NPs obtains in this study to the commercially available one. It could be noticed that this route is cheap and eco-friendly. This waste derived high purity low-cost nano silica is used here to fabricate the silica foam.

Table 4.3 Cost estimation of nano silica synthesis per kg using RHA as source

Raw materials used			Energy			
Name	Cost per kg	Unit price*	Name	Cost per kg	Unit price	Labour cost + others
Rice husk ash	0	0	Magnetic stirring and oven	(3+4) $	0.15 $ per KW	
NaOH pellet	9.8 $	5.2 $ per kg				
HCl solution (1N)	13.5 $	5.4 $ per L				
23.3 $			7 $			7 $
Total extraction cost of nano silica per kg ~ 37.3 $						

* https://www.lobachemie.com/flipbooks

4.3.2 Characterization of 7.5 wt.% solid containing sol

The waste RHA derived sol is appeared in white color. The pH value of the sol is about ~9. When the sol is heat-treated above at 1200°C/1h, it is given around 7.5 wt.% of solid content, which retains about 99.32 wt.% of amorphous SiO_2. Table 4.4 shows the cost estimation of 7.5 wt.% solid containing sol production per litre through the alkali extraction method from RHA as ingredient. Estimated cost of 7.5 wt.% solid (~22 nm average silica particles) containing sol is around 2.86 $ per litre. Subsequently, the cost of commercially available silica sol in market is 0.5$ to 52$ per litre, depends on the solid content, purity and particle size of the silica (Sigma-Aldrich, LUDOX® AS-30 colloidal silica; Colloidal silica import data). It is concluded that this waste derived high purity (99.32 %) silica sol from alkali extraction route is eco-friendly and cheaper compare to its present available aspects.

Table 4.4 Cost estimation of silica sol (~7.5 % solid) synthesis per litre using RHA as source.

Raw materials used			Energy			
Name	**Cost per kg**	**Unit price***	**Name**	**Cost per kg**	**Unit price**	**Labour cost + others**
Rice husk ash NaOH pellet HCl solution (1N)	0 0.74 $ 1.02 $	0 5.2 $ per kg 5.4 $ per L	Magnetic stirring and oven	(0.05+0.05) $	0.05 $ per KW	
	1.76 $			0.10 $		1 $
Total extraction cost of silica sol per litre ~ 2.86 $						

* https://www.lobachemie.com/flipbooks

4.3.3 Characterization of slurry

The rheology characteristic of the slurry is important in this study for the fabrication of crack-free green foam. For the synthesis of in-situ mullite ($3Al_2O_3 \cdot 2SiO_2$) foam, 7.5 wt.% silica-containing RHA derived sol is used with a stoichiometric amount of reactive alumina. The amount of solid content (7.5 wt.%) is optimized to produce crack free foam sample. This sol (without extra water) is supplied the desired flow properties with 0.5 wt.% deflocculant for casting purposes. The slurry is retained around ~22 wt.% of solid content and attributed crack-free green foam during the casting in POP. Figure 4.5 shows the flow curve of this slurry at room temperature. The slurry appears to be a pseudoplastic fluid, as displayed in Figure 4.5(a). It exhibits shear-thinning behaviour due to the presence of an inter-particle

network (-Si-OH), which gradually broke down and showed low viscosity with increasing shear rate. This characteristic can be confirmed plotting the shear stress against shear rate, as shown in Figure 4.5(b). The slurry shows slightly high viscosity, which may be due to the presence of nanoparticles containing sol that provides comparatively large surface areas for particle-to-particle interaction. The irregular particle shape of alumina may be another reason for high viscosity for low solid content (22 wt.%) because it creates difficulty for particles to slide over one another. The specific gravity of slurry and pH value is around 1.55 gm/cc and 8.2, respectively.

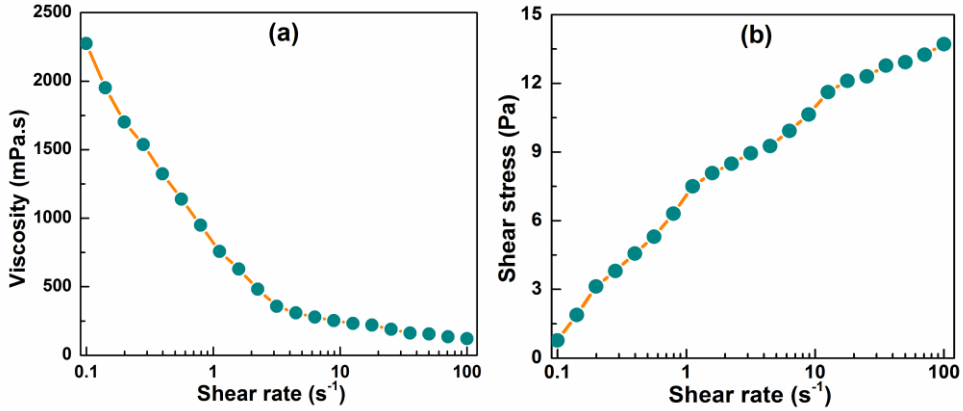

Figure 4.5 Flow curve of the slurry.

4.3.4 Characterization of silica foam

Figure 4.6 shows the XRD pattern of silica foam specimens. It confirms that foams synthesized at low temperature, i.e., 400, 500 and 550°C contain silica in amorphous form only due to lack of any sharp peak in the pattern. However, at 600°C foam sample is composed of some infirm peaks, which demonstrates that the partial crystallinity is formed in the silica. It can be observed that silica synthesized at 600°C is a combination of amorphous broad band, polycrystalline quartz, and low-temperature cristobalite. It may attribute to very slow heating and cooling rate of nanoparticles containing specimens. This is also verified through the DTA image of SiO_2 (Figure 4.4), i.e., after 550°C the silica starts to crystallize.

The AP and BD of the silica foam specimens are illustrated in Table 4.5. It is depicted that the samples are highly porous and it depends upon the compaction of the samples and pore-forming temperature. The pores are formed in the silica matrix through two mechanisms,

which are graphically presented in Figure 4.7. Low compaction is the main reason for the foam formation and causes numbers of voids in the structure. Therefore, a loose structure of silica is formed. However, the porosity is slightly reduced with increasing compaction from 31.20 to 62.40 MPa, due to increase in contact areas between the silica NPs. Another mechanism is the evaporation of absorbed and adsorbed water from the system. With increasing temperature, water is removed in the form of vapour and the pores are formed in the silica foam. Therefore, the porosity increased from 400 to 550°C may be due to the evaporation of adsorbed water molecule, as shown in Figure 4.4. At 600°C, the porosity of f-7 and f-8 specimens is lower, compared to f-5 and f-6, respectively. It may be ascribed to diffuse of silica NPs between each other. Therefore, pore volumes are reduced in the silica matrix.

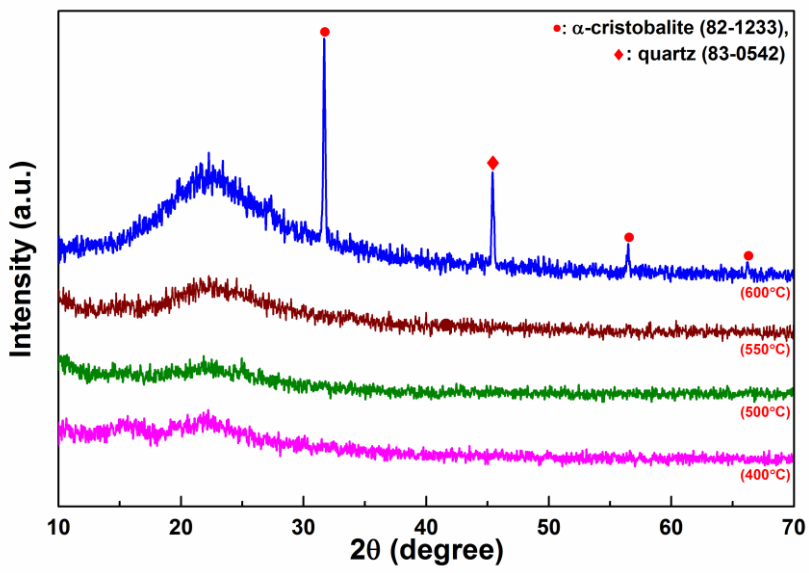

Figure 4.6 XRD patterns of silica foam specimens at different temperatures.

Table 4.5 Apparent porosity, bulk density, and cold crushing strength of the foam specimens.

Samples	Apparent porosity (%)		Bulk density (gm/cc)		Cold crushing strength (MPa)	
	Mean	s.d.	Mean	s.d.	Mean	s.d.
f-1	72.12	1.23	0.573	0.028	1.73	0.13
f-2	66.14	1.08	0.651	0.019	2.05	0.24
f-3	74.09	1.03	0.574	0.020	1.63	0.19
f-4	70.43	0.96	0.640	0.023	1.85	0.24
f-5	75.82	1.15	0.531	0.021	1.54	0.17
f-6	71.42	1.43	0.608	0.034	1.68	0.26
f-7	73.04	1.57	0.591	0.038	1.71	0.28
f-8	70.85	1.08	0.637	0.018	1.84	0.26

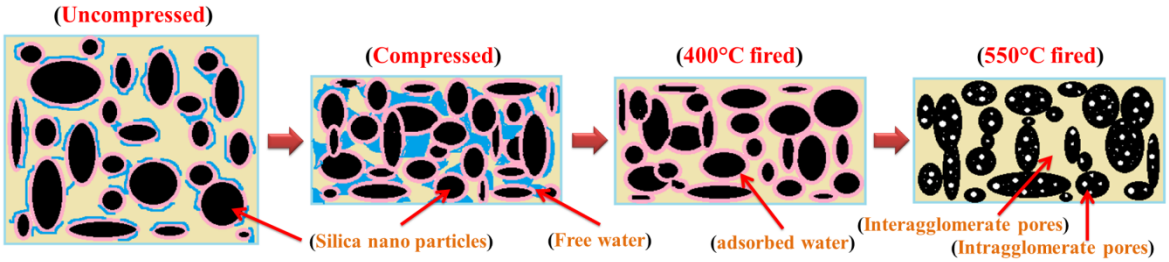

Figure 4.7 Pore forming mechanisms of silica foam specimens.

Figure 4.8(a-b) shows the SEM micrograph of f-5 and f-7 specimens, respectively. Images of different magnification (200, 10000, and 400000X) for f-5 sample are shown in Figure 4.8(a). It can be observed that the sample is highly porous and loose structure. The shape of the pores is irregular, and the size varies from 10 nm to 5 µm. These asymmetric shape pores may be formed due to lack of arrangement of silica NPs and low synthesis temperature. Figure 4.8(a) shows the two different types of pores. One is micro size pores, which may be formed due to low compaction and removal of physical water. Evaporation of chemically bonded water and lack of diffusion kinetics between the silica NPs are another reasons for pore formation, i.e., nano-size pores. Sample f-7 also shows a highly porous structure in Figure 4.8(b). However, the microstructures of f-5 and f-7 could not show any significant changes in SEM images due to a slight difference in porosity (2.78 %) between them.

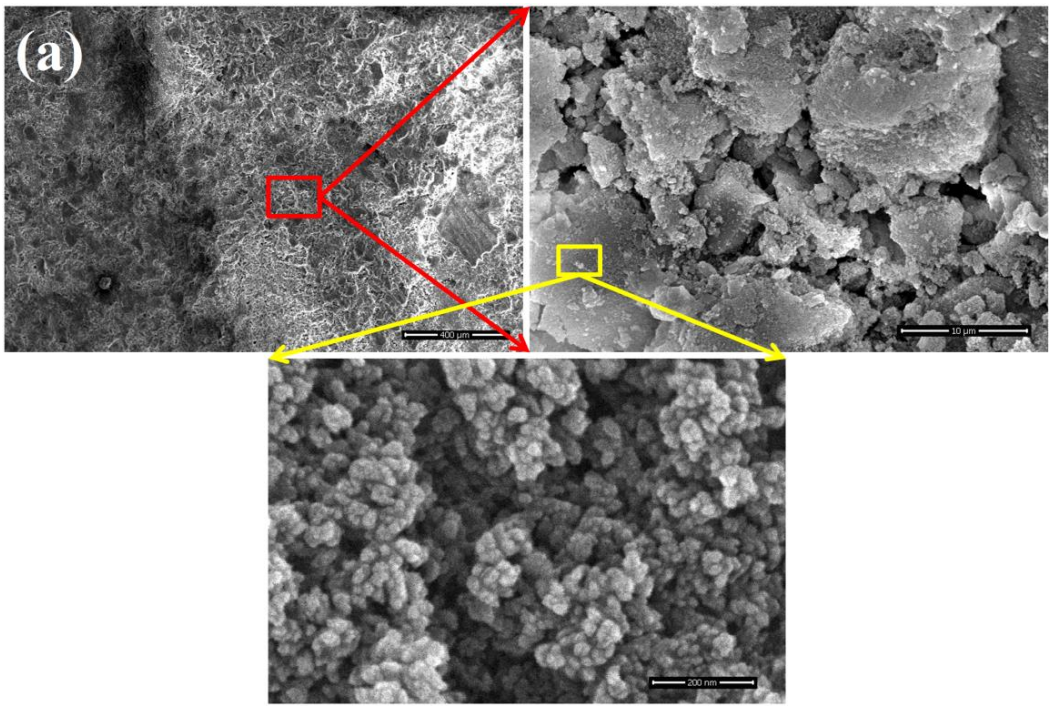

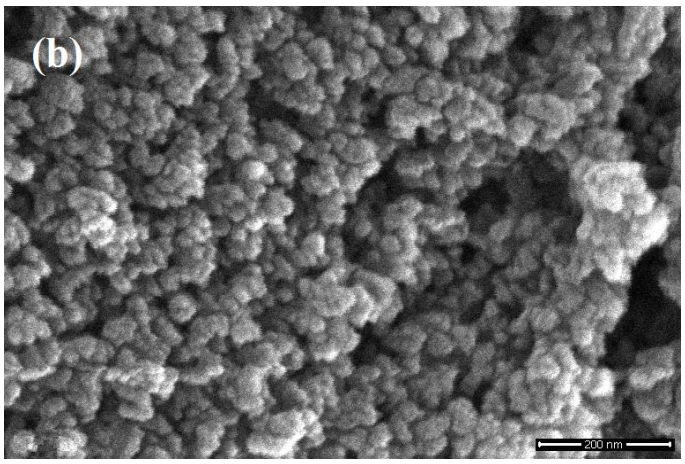

Figure 4.8 SEM images of (a) f-5 and (b) f-7 specimens.

It is highly desirable to perform an in-depth analysis of the surface properties of a material with potential applications as porous ceramics. In this regard, N_2 adsorption-desorption isotherm of the presented silica foam nano pores are measured after a pre-examination treatment at 100°C and analyzed according to Brunauer-Emmett-Teller (BET) and Barrett-Joyner-Halenda (BJH) techniques. Figure 4.9 shows the measured N_2 adsorption-desorption isotherm resemble of the highest porous (AP) specimen, i.e., f-5, which is close to the typical type-II curve of the IUPAC classification (Sing *et al.*, 1985) with H4 type hysteresis. It suggests that the presented silica foam comprises a mesoporous surface structure limited by micro and macro pores, which is supported by the pore-size distribution, as shown in the inlet and clearly showing a majority of pores are within a size range of 2-50 nm. A percentage mesopores of 90.5 % is estimated by considering the volume of mesopores (2-50 nm) over the total pore volume. Additionally, the surface area (S_{BET}), total pore volume and mean pore diameter of the presented silica foam is measured to be 260.57 $m^2 g^{-1}$, 1.3849 $cm^3 g^{-1}$ and 21.259 nm, respectively. It clearly displays that the presented silica foam is embraced with high physisorption properties.

The mean values of CCS of silica foam specimens are tabulated in Table 4.5. It can be seen that the CCS values are decreased with the increasing foam forming temperature. Typically, it occurs due to the increment in the porosity of the brittle body. Porosity in the brittle material is induced a number of crack propagation sites (Vu *et al.*, 2011).

Therefore, less amount of stress is required for breaking the specimens. However, high temperature (600°C) synthesized samples show quite high CCS values. It may occur due to the diffusion of silica NPs to each other at around 600°C and results to the enhancement of CCS values. A comparable study of strength values of silica foam in different studies are shown in Table 4.6. It can be observed that this low-temperature synthesis foam samples show a sustainable mechanical strength. It may be attributed to both small particle size of silica as well as a small size of maximum pores (<50 nm).

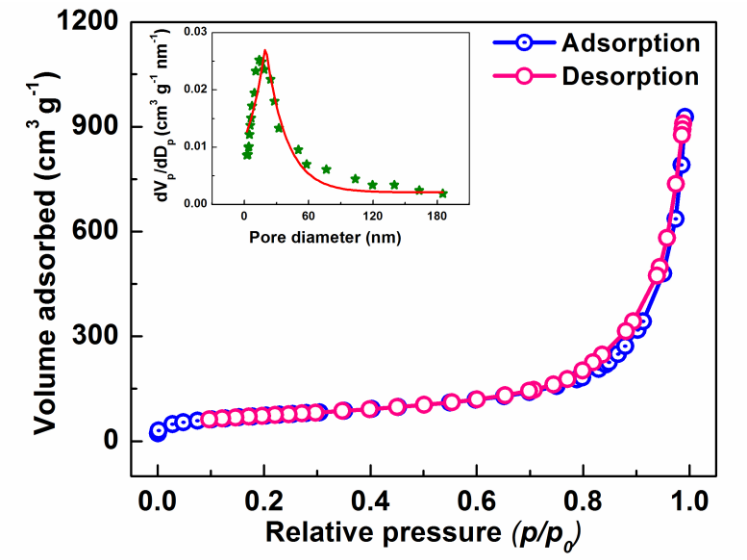

Figure 4.9 N_2 adsorption-desorption isotherm of f-5 foam specimen.

Table 4.6 Comparison of porosity and strength values of silica foam in several studies.

Process	Synthesis temperature (°C)	Apparent porosity (%)	Strength (MPa)	Reference
Steam heating	1150	90	0.3 (CCS)	(Verma *et al.*, 2012)
Mechanical Foaming	1000	66	2.4 (Bending)	(Tomita *et al.*, 2004)
Gel-casting	1300	77	1.4 (CCS)	(Jardim *et al.*, 2016)
Control pressure & temperature	550	76	1.54 (CCS)	Our study

4.3.5 Characterization of mullite foam

Figure 4.10 illustrates the DTA-TGA curve of the dried mixture containing stoichiometric (3:2) amount of reactive alumina and silica (~7.5 wt.% solid containing dry sol) to evaluate the possible mullite formation mechanism. The TGA curve depicts two distinct weight losses from room temperature to 510°C. The first weight loss (~4.5%) up to 170°C is observed due to the elimination of absorbed water from the mixture. Next, weight

loss (~6%) at 230°C to 510°C may be attributed due to the breaking of Si–OH bonds, presented in the silica sol (Liu *et al*., 2007). Consequently, both weight losses are associated with endothermic peaks in the DTA curve. Further, no weight changes are detected in the TGA curve up to 1300°C. However, first exothermic peak at 770°C to 940°C in the DTA curve may be related to the transformation of the amorphous to crystallization of sol containing nano-silica (Munasir *et al*., 2018). The next exothermic peak is detected at around 1030°C. It may be ascribed due to the combination effects like transformation of alumina phase and the formation of Al-Si spinel or nucleation of mullite phase (first step mullite) (Okada *et al*., 2003; Lamouria *et al*., 2016). At high temperature, wide range of exothermic peak at 1110°C to 1300°C (center at 1250°C) may be indicated the crystallization reactions of second step mullite (Janackovi *et al*., 1996; Bhattacharyya and Singh, 2016).

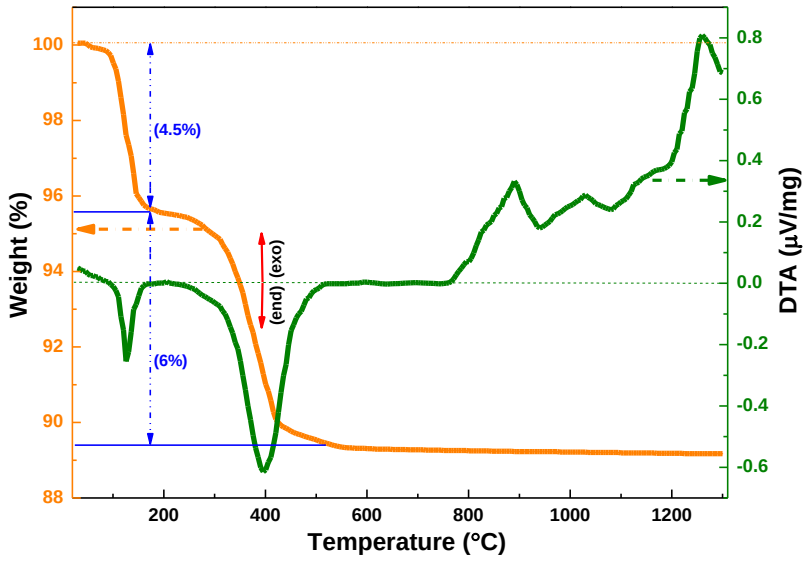

Figure 4.10 DTA-TGA curves of reactive alumina and silica-sol mixture.

Figure 4.11 illustrates the XRD pattern of 1100°C, 1200°C, 1250°C, 1300°C and 1400°C fired casting mass, which contains 2:3 molar ratio of silica (~7.5 wt.% solid containing sol) and reactive alumina. It detects that at 1100°C and 1200°C, sol containing amorphous silica is totally converted into a crystalline form of silica, i.e., cristobalite (JCPDC card number: 76-0937) and a certain amount of mullite phases (JCPDS card number: 06-0258) with unreacted alumina (JCPDS card number: 02-1420). However, significant numbers

of mullite peaks are observed at 1250°C, whereas the numbers of alumina and cristobalite peaks are disappeared in the XRD pattern (Figure 4.11). The maximum intensity peak is located at ~26.40°, which confirms the mullite dominating phase for 1250°C fired system (Janackovi *et al*., 1996). At 1300°C, no diffraction peaks are found corresponding to the alumina and cristobalite phases in the system. They are converted into mullite through the diffusion-reaction of Al^{3+} ions from alumina to the nano-silica (Okada *et al*., 2003). Thus, all peaks in Figure 4.11 (1300°C) are corresponded to the crystalline phase of mullite. It suggests that this system is able to form pure mullite at 1300°C and above. The RHA derived sol containing nano-silica may be the reason for the formation of single-phase mullite at low temperature (Ding *et al*., 2007; Wang *et al*., 2016; Vijayan *et al*., 2017). The mullite formation mechanism with sol containing nano-silica (~22 nm) and reactive alumina (<1 μm) is graphically represented in Figure 4.12. The alumina particles are coated with the silica nanoparticles due to huge size difference between both the reactants. Therefore, the number of diffusion sites for Al^{3+} ions into silica is increased due to the high surface area of nano silica and the diffusion distance for Al^{3+} ions is also low because of the low volume of silica particle. Therefore, the activation energy for mullite formation may be decreased. It is attributed to the mullitization at low temperature, i.e., 1250°C and above. Thus, other characterizations of the foams are investigated with 1250°C (combination of mullite and unreacted parent ingredients), 1300°C, 1350°C and 1400°C fired specimens as they are retained mostly crystalline in-situ mullite phase.

Figure 4.13 displays the SEM images of fractured sections of the foam specimens, which only contains a crystalline phase of mullite for 1300, 1350 and 1400°C fired specimens. The samples are highly porous like foamy structure. However, pores have no particular shape or size, mostly are irregular and inter-connected to each other. The pores sizes are varied from 100 nm to 6 μm for 1300°C fired samples. The size and number of pores are decreased with increasing firing temperature. The formed mullite grains also have no

specific shapes. It may occur due to large size differences of the sol containing silica (~22 nm) and alumina (<1 μm). Consequently, the growth of mullite in certain directions may be inhibited, and nearly spherical to unevenly shaped mullite is formed. Some needle-like mullite grains are also observed in the high magnification SEM image, and its number is increased with increasing firing temperature. High temperatures may supply more energy in the system to overcome the activation energy boundary for growing of mullite in a particular direction (crystallographic c-axis).

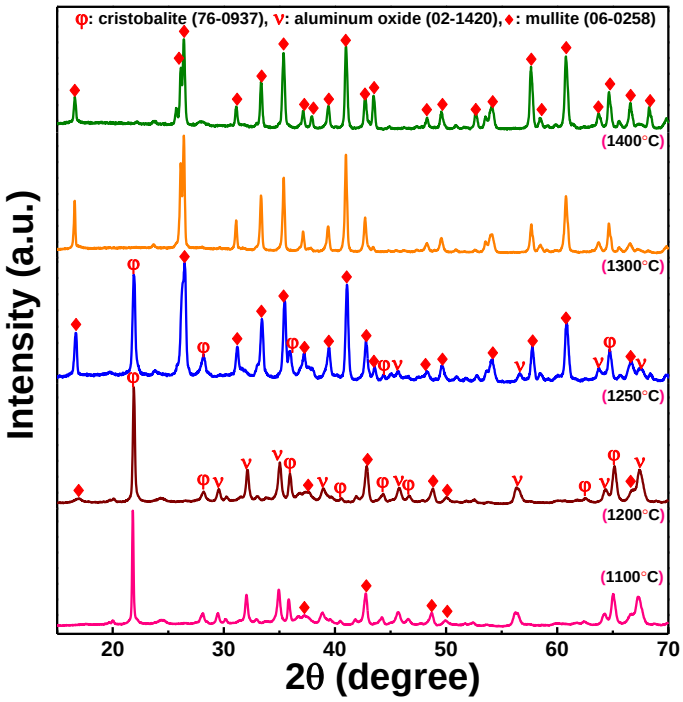

Figure 4.11 XRD pattern of 1100°C, 1200°C, 1250°C, 1300°C, 1350°C and 1400°C fired foam specimens.

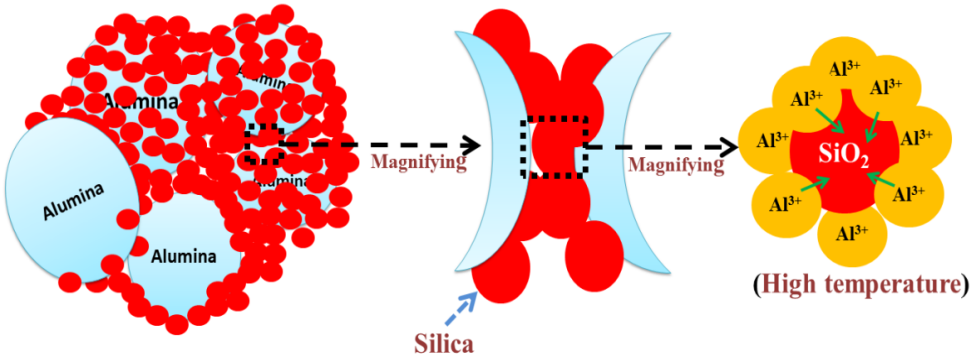

Figure 4.12 Schematic representation of mullite formation reaction mechanism with reactive alumina and sol containing nano silica.

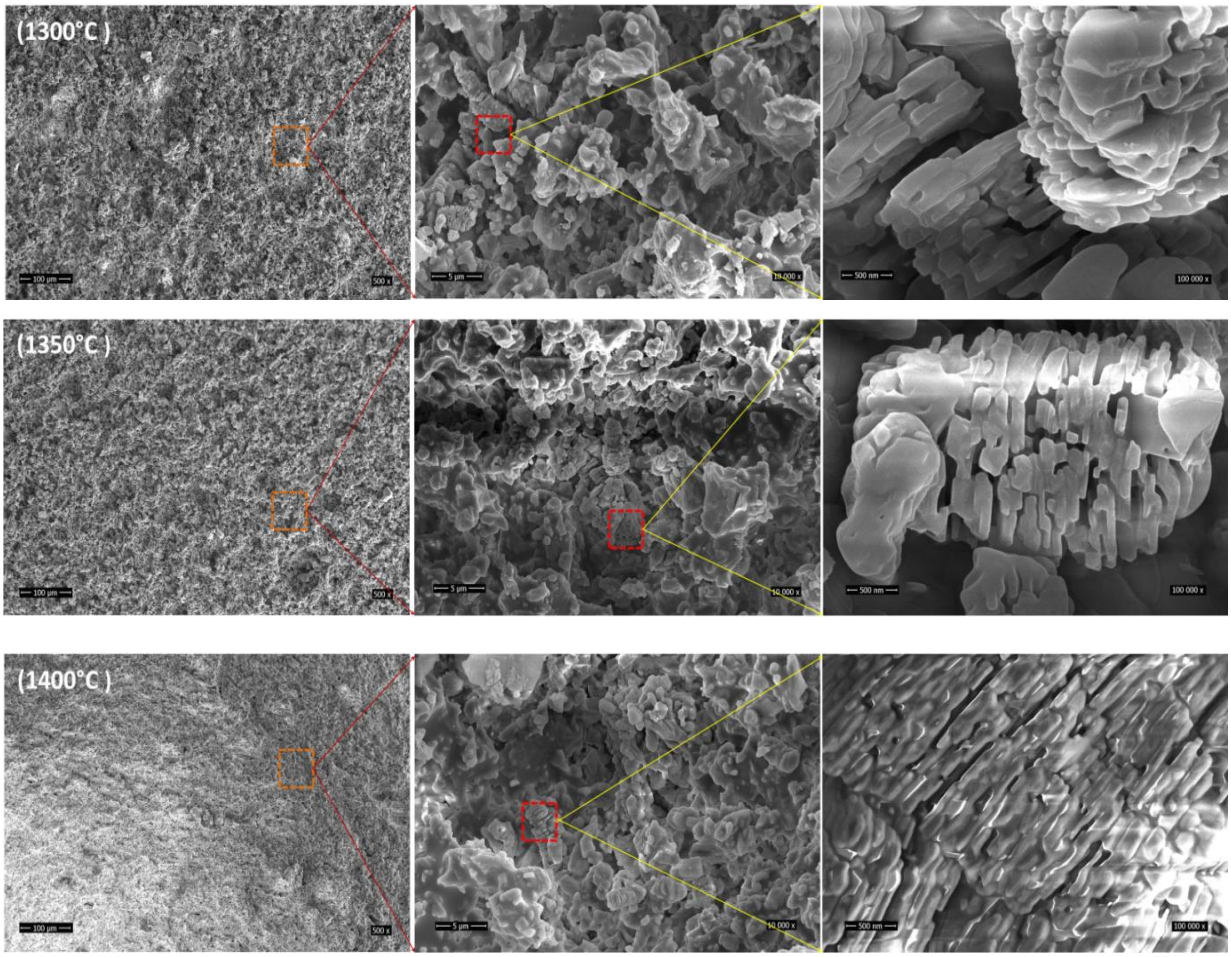

Figure 4.13 SEM micrograph of 1300°C, 1350°C and 1400°C fired mullite foam samples.

The AP, closed porosity, BD and volume shrinkage of the mullite foam samples are illustrated in Table 4.7. It is shown that the foam specimens derived through slip-casting are highly porous without using any pore-forming agent or additive. The pores are generated in the body through the removal of two different types of water from the system, i.e., physical (water) and chemical (hydrated silica containing water) bonded water. These mechanisms are graphically described in Figure 4.14. During casting, water is absorbed from the casting slurry by the POP mould and a layer (casting mass) is formed inside into the cavity of the POP mould. Throughout this process, some pores may be formed in the casting mass due to a lack of packing arrangement of alumina and silica particles. Moreover, the possibility has presented some amount of unabsorbed physical water in the inter-granular spaces of the particles. This water is removed during the drying process at 110°C and creates more porosity in the green body. AP of the dry casting sample is 79.24 %. The chemically bonded water is

eliminated through the equation 4.1 after 450°C during firing process (Liu *et al*., 2007). This effect may also be created new pores in the system but, 1250°C fired specimen shows the AP about 73.45 %, which is lower than the dry casting sample. The porosity formation due to the chemically bonded water removal effect may be diluted by the densification phenomena at high temperature with increasing volume shrinkage on the body (Table 4.7). BD and shrinkage value of the foam samples are increased, and AP is reduced with increasing firing temperature. Fully mullite containing 1300°C and 1350°C fired specimens are retained 71.21 % and 67.73% AP, respectively. However, further increasing firing temperature the porosity is reduced drastically. It may be attributed due to the diffusion of mullite grains (formation of needle shape) to each other as observed in the high magnification SEM image for 1400°C fired samples (Figure 4.13). The AP and volume shrinkage of 1400°C fired specimens is 57.48 % and 16.44 %, respectively. Conversely, the closed porosity is slightly increased due to the higher rate of grain-growth through the different densification kinetics with increasing firing temperature.

$$Si(OH)_4 = SiO_2 + H_2O \uparrow \qquad (4.1)$$

Table 4.7 Apparent porosity, closed porosity, bulk density and volume shrinkage of mullite foam specimens.

Samples	Apparent porosity (%)		Closed porosity (%)	Bulk density (gm/cc)		Volume shrinkage (%)	
	Mean	s.d.		Mean	s.d.	Mean	s.d.
110°C	79.24	2.04	-	-	-	-	-
1250°C	73.45	1.17	-	0.731	0.023	12.67	0.52
1300°C	71.21	1.09	4.78	0.745	0.034	13.29	0.70
1350°C	67.73	1.13	5.93	0.817	0.027	14.07	0.65
1400°C	57.48	1.04	7.35	1.092	0.019	16.44	0.89

Figure 4.15 shows the CCS of before and after fired foam specimens. At 110°C dry sample is shown sustainable strength. It may be developed due to the present of siloxane bonds (Si-O-Si) and silanol groups (Si-OH) in the system. The strength value of the foam specimens is immensely increased after the firing at high temperatures. It may be happened due to the week sol bonds, which are replaced through the strong ceramic bonds. The strength

of the porous, brittle solids depends on the number of pores, size, and interconnectivity of the pores. Therefore, purely mullite containing 1300°C fired sample shows low strength value than other mullite containing samples (1350°C and 1400°C) because it has high porosity (Table 4.7) and a number of interconnecting pores (Figure 4.13). Generally, the CCS performs with the porosity as an inverse manner, i.e., high porosity ascribes a low CCS. It induces a number of promising cracks generating sites in a brittle body and helps to its propagation (Heriyanto *et al*., 2018). Conversely, 1400°C sample exhibits high strength because of low porosity with the formation of more amount of mullite whisker (Figure 4.13). It has an interlocking structure and enhances the strength effectively.

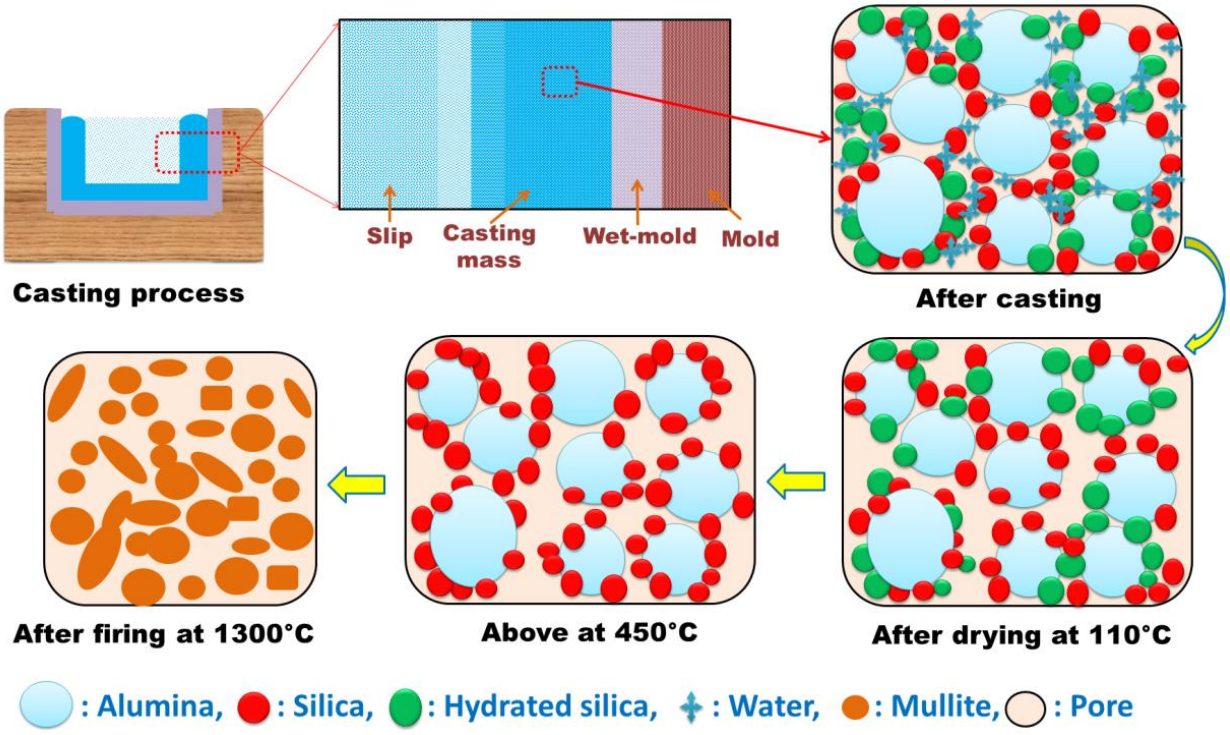

Figure 4.14 Schematic representation of pore formation mechanism of mullite foam through slip-casting.

Figure 4.15 also displays the thermal conductivity (κ) of the foam specimens at room temperature. It is found that 1250°C fired samples exhibit higher κ than 1300°C fired foam samples. It may be ascribed due to the presence of some unreacted alumina in the system (Figure 4.11). Alumina has more κ than the mullite phase (Makeitfrom, 2018). On the other hand, κ of the mullite foams are increased from 0.153 W/m·k to 0.186 W/m·k with increasing

firing temperature from 1300°C to 1400°C. Generally, the κ is increased with decreasing porosity in the materials. Pore size and grain orientation are also affected the κ. Therefore, κ is effectively increased for high-temperature foam samples because of the reduction in number of pores and pore volumes in the system.

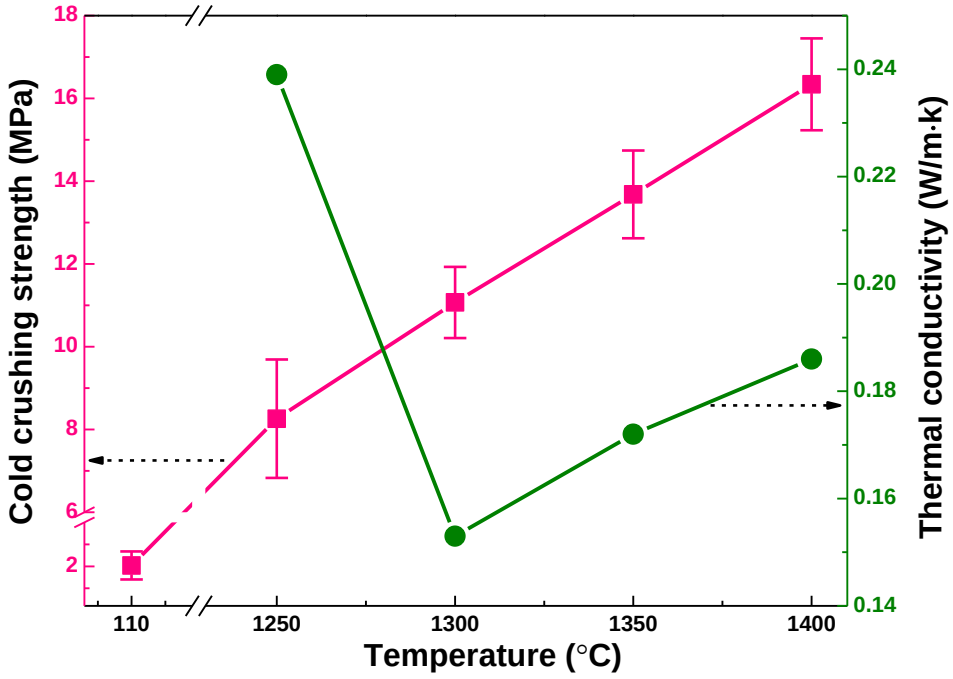

Figure 4.15 CCS and thermal conductivity of foam samples at different temperatures.

From the evaluated characteristic of the foam specimens, 1300°C fired sample shows optimum properties as mullite foam. The key properties (strength and porosity) of this mullite foam sample are compared with the results obtained from the other studies (Table 4.8), where, the porous mullite ceramics are fabricated through different processes and different ingredients. It can be observed that the acquired synthesis process for this study is the most economical and eco-friendly compare to its properties. The used raw materials in this work are also inexpensive. The slip-casting process is very simple than other advanced techniques like gel casting, foam casting, and freeze casting, etc. Any pore-forming agent or pore stabilizer is also not used in this study. Therefore, it has no propensity to generate any greenhouse gases like CO_2 throughout the foam formation and the synthesizing temperature is also low compared to another studies.

Table 4.8 Comparison of the properties between 1300°C fired mullite foam sample with other studies.

Processing method	Main raw materials	Pore former	Firing Temperature (°C)/ time (h)	Porosity (%)	Cold crushing strength (MPa)	Reference
Slip casting	Active alumina, RHA derived sol	-	1300	75.99	11.07	Present work
Foam-gelcasting	Commercial mullite	$CaCO_3$	1300	79.07	5.52	Ge *et al.*, 2018
Starchconsolidation casting	Commercial mullite	Starch	1400/2	64	-	Talou *et al.*, 2015
Freeze-casting	Kaolin, alumina	-	1500/3	83.40	0.49	Wang *et al.*, 2016
Foam-gelcasting	Commercial mullite	Triethanolaminelauryl-sulfate	1600/2	76	15.30	Deng *et al.*, 2015
Gelcasting	Commercial mullite	Fly ash, cenosphere (50 wt.%)	1200	72	11.50	Qian *et al.*, 2014
Direct-foaming	White clay, alumina	-	1500/3	82.60	0.55	Zhou *et al.*, 2018
Gelation freezing	Kaolin, aluminum hydroxide	-	1500/2	90	8.1	Fukushima *et al.*, 2016
Thermo-foaming	Alumina, silica	Sucrose, magnesium nitrate	1600/2	96.28	0.28	Vijayan *et al.*, 2017
Gel freeze drying	Aluminumiso-propoxide, ultrafine silica	-	1600/4	88.60	1.52	Ding *et al.*, 2007
Starch consolidation casting	Fly ash, aluminum hydroxide	Starch	1550/4	55	100 (bending)	Li *et al.*, 2012
Freeze-gel casting	Coal fly ash, alumina	Polyurethane sponge	1400	77.50	7.5	Lee *et al.*, 2013

4.4 Summary

The high purity silica NPs and silica sol was successfully synthesized via the alkali extraction route from the waste RHA. The average particle size of silica is less than 50 nm. The estimated cost of silica NPs and 7.5 wt.% solid containing sol is around ~37.3 $ per kg and ~2.86 $ per litre, respectively.

Silica foams with above 70% of open porosity are successfully prepared without using any additive or pore forming agent. The pores are formed in the foam through control compaction and evaporation of absorbed and adsorbed water in a silica matrix. The microstructures of the foam specimens show the presence of asymmetric, irregular interconnected pores, and the size varies from 2 nm to 5 μm. Porosity also varies with the compaction and foaming temperature. The obtained foam specimens show the significant

CCS at around 1.54 MPa. The promising results (75.82% AP and 1.54 MPa CCS) of foam specimens confirm that the possibility of silica foam fabrication from RHA extracted nano silica through control compaction and low foaming temperature.

The stoichiometric amount of reactive alumina and 7.5 wt.% silica-containing sol with 0.5 % deflocculant is prepared 22 wt.% of solid retaining slurry, which is able to synthesize crack-free green foam through slip-casting method. Sol containing nano-silica is ascribed the mullite formation at low temperature, i.e., 1250°C and above. Mullite foam with 75.99 % total porosity and 11.07 MPa of CCS is successfully synthesized at 1300°C without affecting the environment. The microstructure of the mullite foam sample displays the presence of irregular, asymmetric, interconnected pores with size from 100 nm to 6 μm. The obtained results are confirmed that the possibility of mullite foam synthesis with economically at low temperatures using RHA derived sol through slip-casting process for ceramic industries.